



Article

The Gavkhouni Wetland Dryness and Its Impact on Air Temperature Variability in the Eastern Part of the Zayandeh-Rud River Basin, Iran

Sara Azadi ¹, Hojat Yazdanpanah ^{1,2,*}, Mohammad Ali Nasr-Esfahani ³ , Saeid Pourmanafi ⁴ and Wouter Dorigo ⁵ 

- ¹ Department of Physical Geography, Faculty of Geographical Sciences and Planning, University of Isfahan, Isfahan 8174673441, Iran; s.azadi@geo.ui.ac.ir
- ² Department of Geography, School of Social Sciences, Faculty of Arts and Science, Capilano University, North Vancouver, BC V7J 3H5, Canada
- ³ Department of Water Engineering, Faculty of Agriculture, Shahrekord University, Shahrekord 8818634141, Iran; mnasr@sku.ac.ir
- ⁴ Department of Natural Resources, Isfahan University of Technology, Isfahan 8415683111, Iran; spourmanafi@cc.iut.ac.ir
- ⁵ Department of Geodesy and Geoinformation, Technische Universität Wien, Wiedner Hauptstrasse 8–10, 1040 Vienna, Austria; Wouter.Dorigo@geo.tuwien.ac.at
- * Correspondence: h.yazdan@geog.ui.ac.ir or hyazdanpanah@capilano.ca; Tel.: +98-313-793-5773

Abstract: The Gavkhouni wetland provides many environmental and economic benefits for the central region of Iran. In recent decades, it has completely dried up several times with substantial impacts on local ecosystems and climate. Remote sensing-based Land Surface Temperature (LST), Normalized Difference Water Index (NDWI) and Normalized Difference Vegetation Index (NDVI) in combination with in-situ data were used to investigate the trend of the Gavkhouni wetland dryness and the associated impact on the variability of local air temperature. The results indicate that the wetland has increasingly experienced drier conditions since the year 2000. The wetland was almost completely dry in 2009, 2011, 2015 and 2017. In addition, the results show that Gavkhouni wetland dryness has a significant impact on local climate, increasing the mean seasonal air temperature by ~ 1.6 °C and ~ 1 °C in spring and summer, respectively. Overall, this study shows that remote sensing imagery is a valuable source for monitoring dryness and air temperature variations in the region. Moreover, the results provide a basis for effective water allocation decisions to maintain the hydrological and ecological functionality of the Gavkhouni wetland. Considering that many factors such as latitude, cloud cover, and the direction of prevailing winds affect land surface and air temperatures, it is suggested to use a numerical climate model to improve a regional understanding of the effects of wetland dryness on the surrounding climate.

Keywords: remote sensing; trend; land surface temperature (LST); NDWI; NDVI; local climate



Citation: Azadi, S.; Yazdanpanah, H.; Nasr-Esfahani, M.A.; Pourmanafi, S.; Dorigo, W. The Gavkhouni Wetland Dryness and Its Impact on Air Temperature Variability in the Eastern Part of the Zayandeh-Rud River Basin, Iran. *Water* **2022**, *14*, 172. <https://doi.org/10.3390/w14020172>

Academic Editor: Zongming Wang

Received: 9 November 2021

Accepted: 29 December 2021

Published: 9 January 2022

Publisher's Note: MDPI stays neutral with regard to jurisdictional claims in published maps and institutional affiliations.



Copyright: © 2022 by the authors. Licensee MDPI, Basel, Switzerland. This article is an open access article distributed under the terms and conditions of the Creative Commons Attribution (CC BY) license (<https://creativecommons.org/licenses/by/4.0/>).

1. Introduction

Wetlands, as aquatic ecosystems, provide a variety of benefits to wildlife and humans in many different ways [1,2]. Some of the services provided by wetlands include reducing greenhouse gasses, regulating climate [3], purifying water, storing pollutants in their soils, and vegetation maintaining water supply [4], providing breeding habitat for various species of fauna, and flora, and biodiversity function [5]. Wetlands are one of the vital micro-components of climate as they have their own specific moisture cycles with aquatic plants [6]. Changing land uses, such as forests, agricultural lands, built-up areas, and land cover, including soil, snow, or water, can affect climate [7].

In recent decades, wetlands have been heavily impacted by anthropogenic activities and climate change [5], lack of an integrated management program for wetlands and the rivers that feed them, droughts, and other factors cause them to dry up.

Land Surface Temperature (LST) as an essential key parameter of the land environment [8], and surface LST in micro, local, regional and global scales [9] is affected by changes in land surface characteristics such as vegetation cover and land use/cover [10]. Therefore, a decrease in the wetland area or reduction of the amount of water in the wetland may be associated with changes in LST. Hence, the study of changes in LST, which plays an important role in the interaction between the surface and the atmosphere [11], is important, especially for aquatic ecosystems in arid and semi-arid regions, which face various natural phenomena such as climate change, drought and also anthropogenic influences. Remote sensing-based LST is a useful tool for studying land surface changes in spatial and temporal terms. Despite the limited ground data, remote sensing techniques are used significantly to understand the changes in land surface properties and also to identify the behavior of climate variables due to the provision of extensive information at high resolution [12]. LST is used in various studies for different scientific purposes, e.g., vegetation and land use/cover changes [13–23], the urban heat island [24–26], drought monitoring [27–31], frost risk [32], land degradation [33,34], hydrological purposes [35,36].

Among the various remote sensing indices, NDWI (Normalized Difference Water Index) is one of the most water practical indices used in many studies to track and predict wetland hydrological changes [37–40]. In addition, NDVI (Normalized Difference Vegetation Index) has been used as a vegetation indicator to investigate changes in vegetation conditions [33,41].

The Gavkhouni wetland located in the eastern part of the Zayandeh-Rud River Basin is fed by the Zayandeh-Rud River. In recent years, the wetland has dried up due to rainfall deficits, severe water shortages, human intervention and manipulation [42], and the transfer of chemical and physical pollutants, which have affected the conditions of the surrounding area and reduced the wetland's services (<https://www.iranaqua.ir>, accessed on 1 August 2021). Due to the lack of in-situ meteorological data to study the air and land surface temperature changes, remote sensing techniques are used to understand the overall state of change in the wetland's region. A few studies, especially using remote sensing data, were conducted for this wetland, such as Mirahsani et al. [43], who focused on drought analysis using SPI (The Standardized Precipitation Index) and VCI (The Vegetation Condition Index) indices, and Shiran et al. [44], who showed the relationship between NDVI and LST and land properties.

A comprehensive understanding of wetland ecosystem services, especially from the ecological point of view, requires knowledge of the interaction between wetland and climatic parameters of the region. Hence, research is needed on the impacts of the Gavkhouni wetland dryness on regional climate variability to make appropriate river and wetland management decisions in this region. Therefore, the main objective of the current study is quantifying the drying out of the Gavkhouni wetland and its impact on air temperature variability over the study area.

2. Materials and Methods

2.1. Study Area

The main feature of the Zayandeh-Rud River Basin, which is located in the most central and arid region of Iran, is the Zayandeh-Rud River (Figure 1a), which originates from the Zagros Mountains in the west at an altitude of 4500 m (32°22' N, 50°04' E) and flows ~350 km to the east to end in the shallow place called Gavkhouni wetland at 1470 m [45]. The study area shown in Figure 1a is located in the eastern part of the Zayandeh-Rud River Basin and focuses on the Gavkhouni wetland and its surrounding area (52°39' E, 32°25' N). The Gavkhouni wetland, which was included in the international Ramsar Convention as an international wetland in 1975 [42] has an area of 476 km² and is situated downstream of

the Zayandeh-Rud River. According to the reports of the Iran Meteorological Organization, the maximum depth of stored water in the wetland is about 80 to 150 cm.

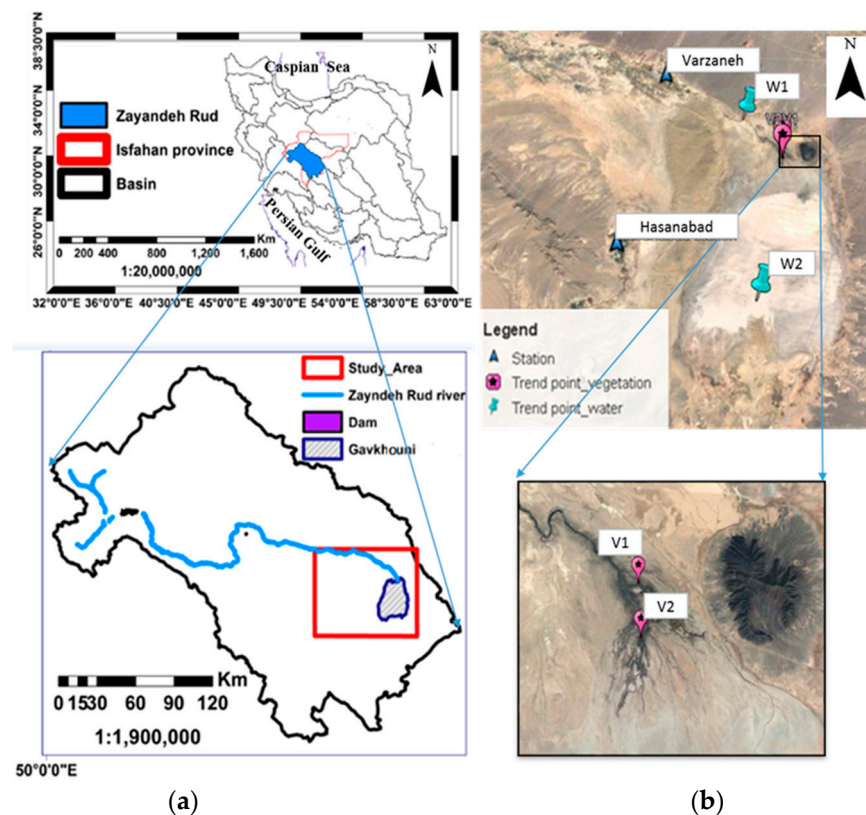


Figure 1. (a) Location of the Gavkhouni wetland and the study area (red boundary) in the Zayandeh-Rud River Basin, Isfahan province, Iran; (b) two meteorological stations and the selected points (W1–W2, V1–V2) for trends of dryness and vegetation cover.

The climate of the Zayandeh-Rud River Basin has a dramatic range. The average rainfall is ~1500 mm and is comprised of snow falling in the west of the basin, and ~110 mm of rain in the eastern parts, including the Gavkhouni wetland [42].

The Zayandeh-Rud River Basin is one of the most populous and industrialized watersheds in the country of Iran [45]. In the past several decades, the water and vegetation of the basin have been highly abundant, resulting in the identification of more than 910 plant species, 390 genera, and 83 families, including native plants, with genetic, medicinal, ornamental, edible, and industrial values. These plants also serve as a natural filtration system (<https://www.iranaqua.ir>, accessed on 1 August 2021). In contrast, the Zayandeh-Rud River has recently been dried up for several years and has turned the wetland into a salt pan, which has negatively affected the climate, environment, life of related organisms and the natural ecosystem of it and the surrounding region. Especially changes in the biological and environmental conditions of the Gavkhouni wetland as the most critical wetland in this arid region, have many different consequences, such as a drastic decline of flora and fauna in the wetland, which has been observed in recent years. Figure 2 qualitatively shows the environmental conditions of the wetland.

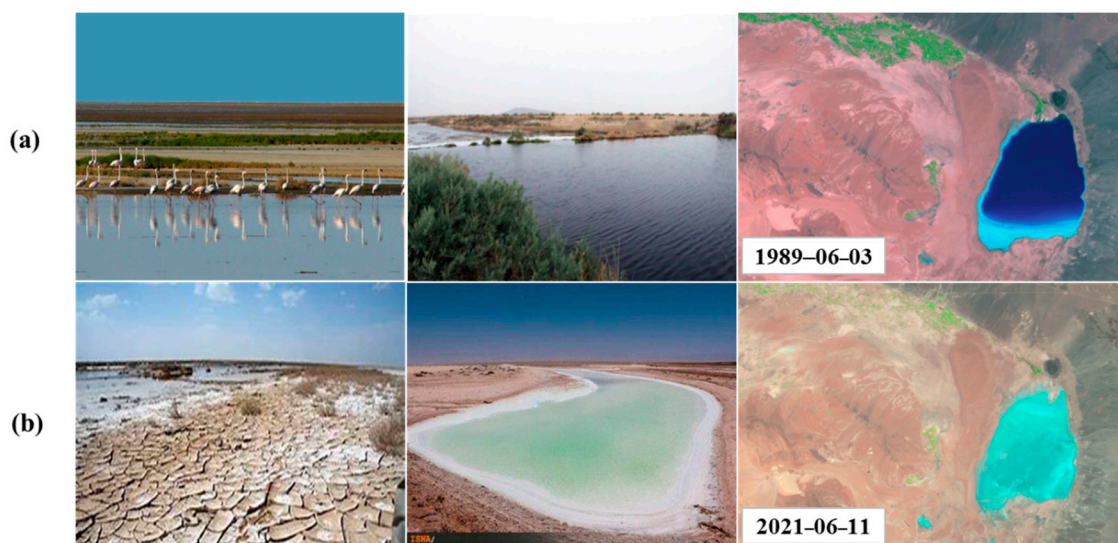


Figure 2. The situation of the Gavkhouni wetland: (a) in the past (before 2000); (b) at present.

2.2. Methodology

2.2.1. Trends of NDWI and NDVI for Presence of Water and Vegetation

The remote sensing data used, and the processing applied for trend analysis were based on the Climate Engine Web Application (<http://climateengine.org>, accessed on 1 August 2021).

For the trend analysis, the values of two spectral indices (NDWI for the presence of water and NDVI for vegetation) in row 38 and path 163 (row and column of the Landsat image tile) were taken from time-series images of Landsat 4 and Landsat 5 (Thematic Mapper; TM), Landsat 7 (Enhanced Thematic Mapper; ETM+), and Landsat 8 (Operational Land Imager (OLI) and Thermal Infrared Sensor (TIRS); OLI/TIRS) at a spatial resolution of 30 m from January 1984 to August 2020.

Initially, the values of the indices were derived, and then the time series trends (linear method), long-term averages for the period 1984–2020, and monthly and seasonal averages were subtracted from the time series to show the overall trends in the drying of wetland and the decrease in vegetation cover in its surrounding area.

As shown in Figure 1b, four points were selected near the Gavkhouni wetland and within the wetland (points W1–W2 and V1–V2 were selected for NDWI and NDVI, respectively). In addition, the monthly time series of river discharge at the Varzaneh hydrometric station (latitude = 32.4236°, longitude = 52.6633° and elevation = 1495 m) as the latest station of the Zayandeh-Rud River before the entrance of the Gavkhouni wetland in the period of 1970 to 2019 were obtained from the Regional Water Company of Esfahan (<https://www.esrw.ir>, accessed on 1 August 2021).

2.2.2. Calculation of LST

The data and the processes used to calculate LST were based on the Earth Explorer application (EE) and an open-source software of remote sensing (QGIS). EE is a web application that allows users to retrieve Earth imagery across all available geospatial data types published by the U.S. Geological Survey (USGS) (<https://earthexplorer.usgs.gov>, accessed on 1 August 2021). According to the overall results of the wetland drying trends (Section 2.2.1), 16 days in four seasons were selected in the last decade, i.e., 2009, 2011, 2015, and 2017 (Table 1), when the wetland was almost dry. In this section, 16 Landsat images were collected from Landsat 5 (TM) and Landsat 8 (OLI/TIRS) with a spatial resolution of 30 m and cloud cover of less than 10% to investigate the spatio-temporal variability of

LST and to show the climate conditions of the studied area. LST variable was calculated according to Equation (1) [46] as follows:

$$T_s = \frac{TB}{1 + \left(\lambda \frac{TB}{\rho}\right) \ln \varepsilon_\lambda} - 273.15 \quad (1)$$

where T_s is the LST in degree Celsius ($^{\circ}\text{C}$), TB is at-sensor brightness temperature (degree Kelvin, $^{\circ}\text{K}$, Equation (2)), λ is the wavelength of emitted radiance for which the peak response and the average of the limiting wavelength [47] will be used, ε_λ is the land surface emissivity calculated from NDVI and Pv as the percent of vegetation calculated using NDVI, NDVImin, and NDVImax, $\rho = h \times c/\sigma$, where h is Plank's constant (6.626×10^{-34} J s), and c is the velocity of light (2.998×10^8 m/s), and σ is Stefan-Boltzmann's constant (1.38×10^{-23} J/K) [48]:

$$TB = \frac{K_2}{\ln\left(\left(\frac{K_1}{L_\lambda}\right) + 1\right)} \quad (2)$$

Table 1. Data sets used to derive LST and Tair_calc (calculated air temperature) maps for the study area and the selected 16 days at 06:48 to 07:03 GMT.

Season	Day	Satellite-Sensor	Time	
			GMT	Local
Winter	17 January 2009	LT05-TM	06:48	10:18
	07 January 2011	LT05-TM	06:53	10:23
	23 January 2011	LT05-TM	06:53	10:23
	09 December 2017	LT08-OLI/TIRS	07:03	10:23
Spring	25 May 2009	LT05-TM	06:51	10:21
	31 May 2011	LT05-TM	06:52	10:22
	12 March 2017	LT08-OLI/TIRS	07:03	10:33
Summer	28 July 2009	LT05-TM	06:52	10:22
	18 July 2011	LT05-TM	06:52	10:22
	27 June 2015	LT08-OLI/TIRS	07:02	10:32
	30 August 2015	LT08-OLI/TIRS	07:03	10:33
	16 June 2017	LT08-OLI/TIRS	07:03	10:33
	04 September 2017	LT08-OLI/TIRS	07:03	10:33
Autumn	16 October 2009	LT05-TM	06:53	10:23
	22 October 2011	LT05-TM	06:51	10:21
	17 October 2015	LT08-OLI/TIRS	07:03	10:33

In the above Equation (2), K_1 and K_2 are the band-specific thermal conversion constants obtained from metadata in $\text{W}/(\text{m}^2 \text{ sr})$, and L_λ is spectral at-sensor radiance in $\text{W}/(\text{m}^2 \text{ sr } \mu\text{m})$ [13].

2.2.3. Calculation of Air Temperature

Air temperature (Tair_calc) variability in the region was derived by a linear regression model between the observed air temperature (Tair_obs) at two available meteorological stations (Varzaneh and Hasanabad, Figure 1b) and the remotely sensed LST product at these locations. The coefficient of determination (R^2) and root mean square error (RMSE) were used to evaluate the accuracy of the model developed for estimating air temperature based on Landsat LST products for the studied area. The equations of these metrics are as follows as Equations (3) and (4) where X_0 is the observed data, and X_s is the simulated data.

$$R^2 = \frac{\sum_{i=1}^N X_0 X_s}{\sqrt{\sum_{i=1}^N X_0^2 \sum_{i=1}^N X_s^2}} \quad (3)$$

$$\text{RMSE} = \sqrt{\frac{\sum_{i=1}^N (X_0 - X_s)^2}{N}} \quad (4)$$

2.2.4. Trend of Observed Temperatures

To understand the effects of the dryness of the Gavkhouni wetland on the temperature of its surrounding geographical areas, according to the maps of LST involving 16 cases, two summer cases were selected in which the wetland was dry and almost wet, respectively. According to the reports of the Iran Meteorological Organization, the prevailing wind direction in Varzaneh is west in winter, spring, and autumn, and east in summer. Therefore, two cases were considered in summertime to obtain an overview of the effect of the wetland dryness on its surroundings, especially in the west toward the northwest parts. Next, the observed air temperatures of the meteorological stations (Varzaneh and Hasanabad) at 06:00 and 12:00 GMT were compared with the long-term seasonal average of observed air temperatures ($T_{\text{air_obs_m}}$) (Table 2 and Figure 1b). Then, the trends of the observational mean monthly minimum ($T_{\text{min_m}}$) and maximum air temperature values ($T_{\text{max_m}}$) were calculated using the non-parametric Mann-Kendall test [49]. The observed monthly air temperature data were collected for the whole of Iran in 40 meteorological stations (including 38 synoptic stations and two combined synoptic-climatology stations), for Isfahan province (four stations including Isfahan, Kashan, Naein, and Varzaneh) and for Varzaneh station, as three areas from 1970 to 2019. Then the data was divided into 1970–1999 and 2000–2019 as two periods before and after 2000 ((based on the river discharge (m^3/s) at Varzaneh station, and the trends of the NDWI and NDVI indices (Section 2.2.1). Finally, the mean value of Sen's slope (the slope in Mann-Kendall trend test), for all 12 months for three areas was derived and compared.

Table 2. Long-term seasonal ** average of observed air temperature ($T_{\text{air_obs_m}}$) in two available stations at 06:00 and 12:00 GMT.

Station *	Winter		Spring		Summer		Autumn	
	06:00	12:00	06:00	12:00	06:00	12:00	06:00	12:00
Varzaneh	4.0	11.9	17.5	23.6	30.6	36.1	17.3	24.8
Hasanabad	5.1	9.0	17.7	22.1	30.0	34.5	17.7	22.0

* Varzaneh (latitude = 32.4° and longitude = 52.66667°) is a synoptic station of Iran Meteorological Organization with data from 2006 to 2020, and Hasanabad (latitude = 32.1387° and longitude = 52.6267°) is a station of Regional Water Company of Esfahan with data from 2003 to 2020. ** Winter: Dec, Jan, Feb; Spring: Mar, Apr, May; Summer: Jun, Jul, Aug; Autumn: Sep, Oct, Nov.

2.2.5. Comparison of Observational Air Temperature in Dryness and Wetness Conditions of Wetland

To identify the difference in air temperature adjacent to the wetland area in two different wet and dry conditions of the wetland, groups of the observational air temperatures in dry and wet conditions were used. To find out the dry and wet conditions, the monthly values of river discharge (m^3/s) at the hydrometric station closest to the Gavkhouni wetland from 1970 to 2020, and the results of the presence of water and vegetation cover (Section 2.2.1) were considered. For this purpose, all available Landsat imagery from 1982 to 2020 was also used to determine the years in which the wetland was full of water or was almost dry. Next, the mean monthly air temperatures of these two situations were compared using the Student's t -test (t test). To eliminate the role of global warming during recent decades (2000s and 2010s), the values of the global warming rate for each season and both the minimum and maximum temperatures were derived using the results of the temperature increase rate or Sen's slope estimator (Section 2.2.4). In other words, to find out the effect of the wetland dryness on air temperature variations in the region, the global warming rate for all data was removed, and the remaining values were used in a paired two-sample t test.

3. Results

3.1. Trends of NDWI, NDVI

Figure 3 shows the time series analysis of NDWI and NDVI values at the selected points (W1; in the river and near the entrance of the wetland (Figure 3a), W2; in the middle of the wetland (Figure 3b), V1 and V2; near the river and the entrance of the wetland, respectively (Figure 3c,d)) between January 1984 and August 2020. In Figure 3, a significant downward trend can be seen at all points, but the long-term average value of NDWI was negative and close to zero, corresponding to the non-water area. While the long-term value of NDVI was positive and close to 0.3, corresponding to shrublands and grassland. In addition, the highest values of NDWI (~ 0.3 , corresponding to the water feature) and NDVI (≥ 0.4) were observed in the 1990s and 1980s (especially in 1988, 1989, 1993, and 1994 for NDWI, and 1997, 1993, and 1994 for NDVI) and during some months of 2008/2009 and 2018/2019 (mainly autumn months). In these years, the maximum values of NDWI (≥ 0.3) at point W1 (within the river near the wetland) were observed in spring (October, November, and December) and then in winter and early spring (January to March). The maximum values of NDWI (≥ 0.5) at point W2 (in the middle of the wetland) corresponded to spring (December, January, February), summer (June), and autumn (November), while the maximum values of NDVI (≥ 0.4) at both point V1 (adjacent to the river near the wetland) and point V2 (adjacent to the river and near the wetland entrance) corresponded to summer and autumn (June to October).

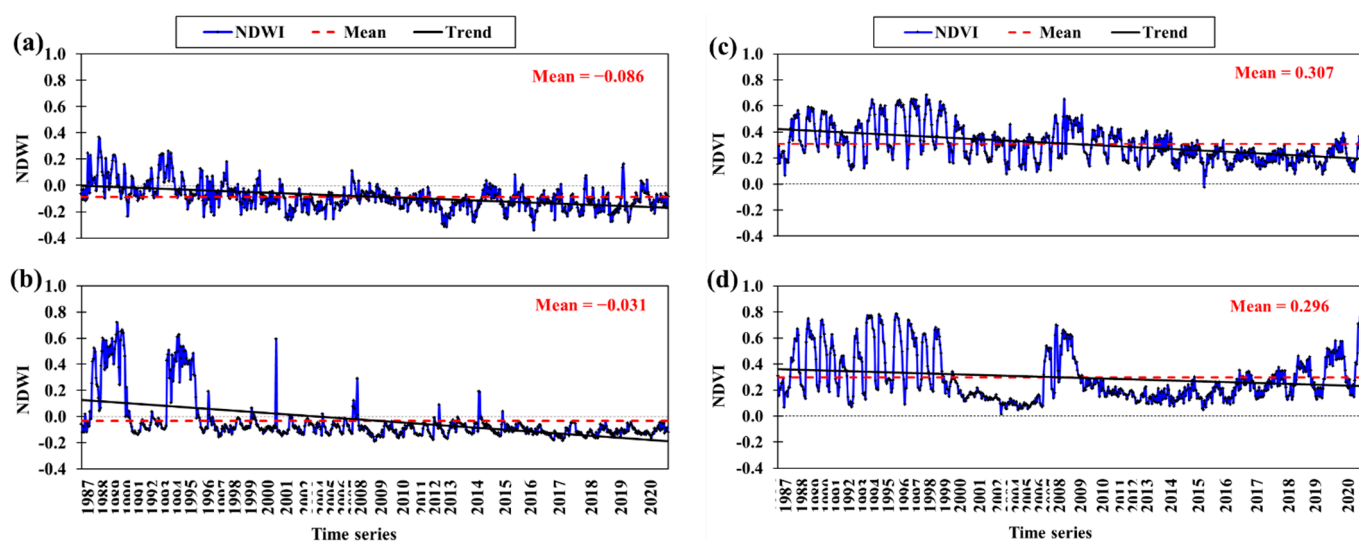


Figure 3. Time series values of NDWI at the selected points: (a) W1; (b) W2, and NDVI at the selected points: (c) V1; (d) V2, from 1984 to 2020.

In the most recent years (especially from 2008/2009 to 2018), the values of NDWI and NDVI were below their long-term averages.

Figure 4 illustrates the seasonal and monthly averages of the NDWI and NDVI indices over the long term at four points. Figure 4a shows that the highest values of the seasonal average of NDWI at point W1 were in autumn, followed by summer, winter, and spring. At point W2 the highest values were observed in winter, spring, summer, and autumn because the Zayandeh-Rud River was dry for a long time and no water flowed to fill the Gavkhouni wetland. While the highest values of NDVI at both points V1 and V2 were in summer, followed by autumn, spring, and winter.

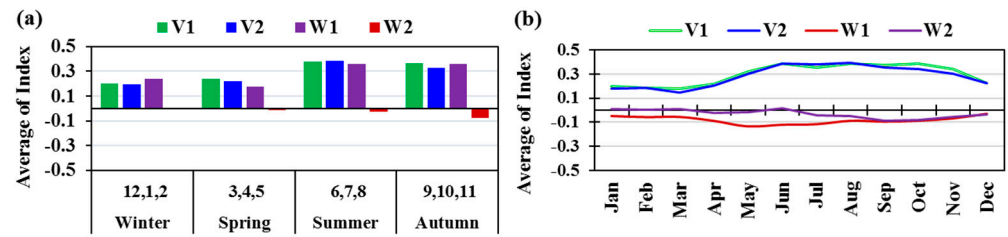


Figure 4. Average of the indices at the selected points: V1 and V2 (NDVI), W1 and W2 (NDWI): (a) Seasonal; (b) Monthly.

Figure 4b shows the monthly average values of the NDWI and NDVI indices over the long-term at four selected points, where the NDWI at point W1 had high values in March, June, and July, while it was observed at point W2 in September and October. The high values of NDVI at both points V1 and V2 were related to June to November (summer and autumn months). As can be seen in Figure 4b, the changes at point W2 were similar to those at points V1 and V2, which means that the wetland (W2) was dry during the summer months (negative values of NDWI). Since the Zayandeh-Rud River (which fed the wetland) was dry, the vegetation covers near the river and the wetland decreased almost with a time lag.

Figure 5 shows the monthly discharge values at Varzaneh as the nearest hydrometric station to the Gavkhouni wetland, from 1970 to 2019. As shown in Figure 5a, the highest discharge values were recorded in spring (especially May, and then April) and winter months (especially December). The highest discharge values were related to 1976, then 1993, 1987, 1988, and 1980 with maximum values of 107, 90.5, 82.5, 64, and 63 (m³/s), respectively. Figure 5a,b shows that most years before 2000 were wet, while the wetland condition after that year was dry.

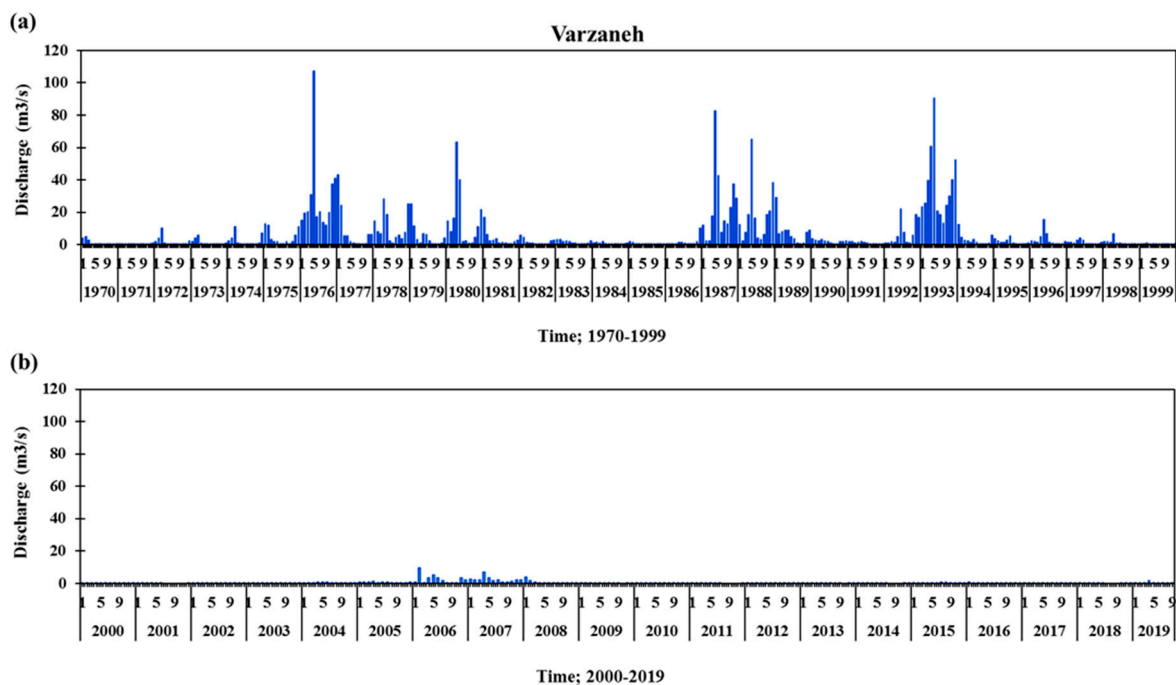


Figure 5. Monthly time series of discharge at Varzaneh hydrometric station: (a) 1970–1999; (b) 2000–2019.

3.2. LST and Tair_calc Spatiotemporal Variations

To investigate the spatial and temporal variations of land surface and air temperatures with a spatial resolution of 30 m over the Gavkhouni wetland and its surrounding area, as

per Figures 3–5, some cases were selected in 2009, 2011, 2015 and 2017, that approximately corresponded to the dry condition of the wetland and the available and usable Landsat imagery. The maps LST and the subsequently calculated air temperature (Tair_calc) are presented and discussed below.

Figures 6 (as an example for summer season) and S1–S3 demonstrate the Landsat LST (°C) at 06:48–7:03 GMT (10:18–10:33 local time) on 16 selected days in summer, winter, spring, and autumn, respectively. In all seasons and on almost all selected days, LST in the wetland was lower than in the surrounding area, also at Varzaneh and Hasanabad stations. In the study area, during winter, spring, summer, and autumn, the areas with the highest values of LST were most prevalent in the outer areas near the wetland corresponding to the sand dunes (as an example shown in Figure 6(e1-1)) and black rock (Figure 6(e1-2)). Some parts of the Gavkhouni wetland, mainly after the entrance, and narrow parts in the east and southeast of the wetland were cooler than other parts, while some parts, especially in the middle and south of the wetland, had a higher temperature class. The minimum values of LST were also observed outside the wetland, for example, some parts in the west of the study area (white rocks in the mountainous part (Figure 6(e1-3))) and some narrow parts near Varzaneh (in the northwest of the wetland) and Hasanabad towns (west) (built-up area (Figure 6(e1-4))) which had high albedo and ultimately decreased the LST values.

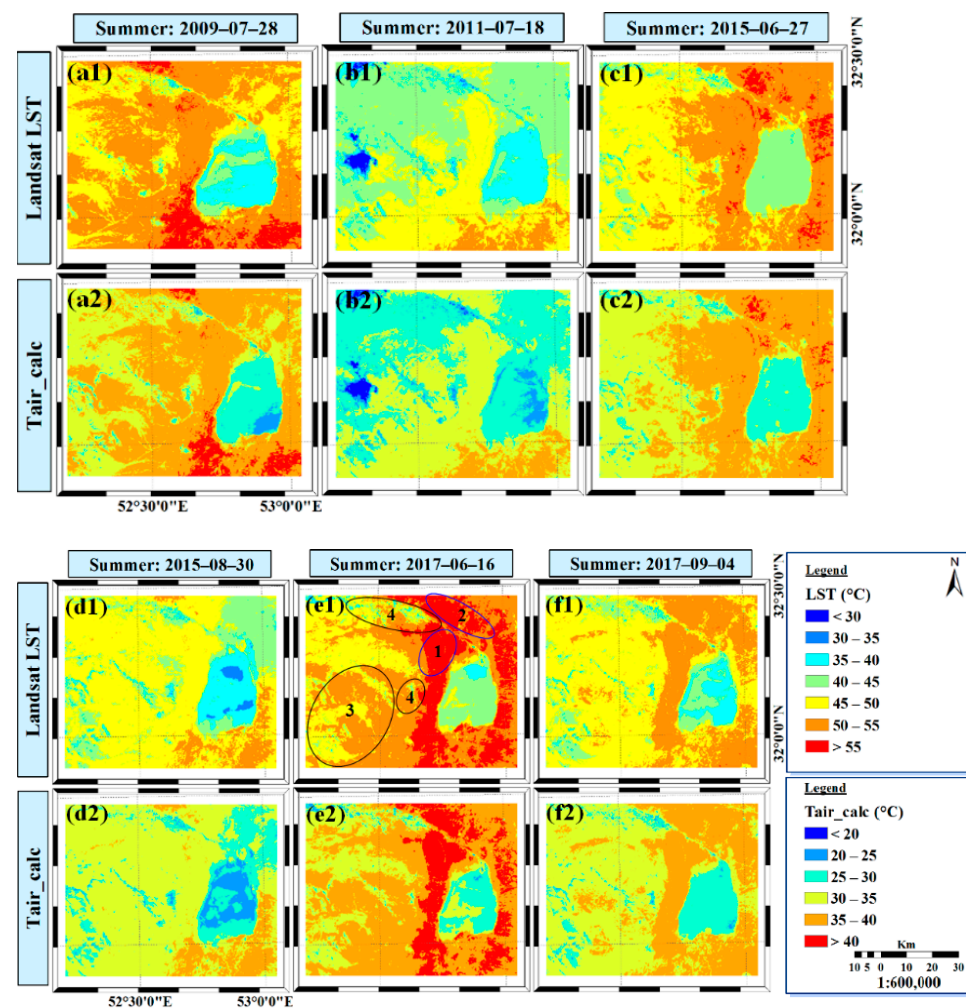


Figure 6. LST and Tair_calc (°C) variability in the study area in summer: (a1,a2) 2009-07-28; (b1,b2) 2011-07-18; (c1,c2) 2015-06-27; (d1,d2) 2015-08-30; (e1,e2) 2017-06-16; (f1,f2) 2017-09-04.

As shown in Figure S4, the calculated air temperature (T_{air_calc}) was obtained using the linear regression between LST and observed air temperature (T_{air_obs}) for the selected 16 days at two stations (Varzaneh and Hasanabad) which showed the strong correlation ($r = 0.97$, $r^2 = 0.94$) and $RMSE = 3\text{ }^{\circ}\text{C}$. The difference between LST and T_{air_obs} in 16 days showed higher values in Varzaneh than the Hasanabad station.

At these two stations, and in all seasons, the values of LST were higher than those of T_{air_calc} and T_{air_obs} . Moreover, the values of T_{air_calc} and T_{air_obs} were close in all seasons except winter, and the $RMSE$ was about $3\text{ }^{\circ}\text{C}$ at two stations.

As shown in Figure S5, the values of LST at Hasanabad were lower than that of Varzaneh station on most of the selected days and months. Figures 6 and S1–S3 also show that in this study area, as with LST (Figures 6 and S1–S3), the lowest and highest T_{air_calc} values were found in almost all the seasons inside and outside the wetland, respectively.

3.3. The Gavkhouni Wetland Dryness Impact

3.3.1. Two Summer Cases

For this purpose, according to Table 2 and Figures 6 and S1–S3, the days 27 June 2015 and 28 July 2009 were selected (Figure 6(a1,c1)) where the maximum and minimum values of LST occurred at 06:00 GMT for the entire wetland and for the entire study area in summer, respectively. These cases also had a wet and dry winter, respectively. Table 2 and Figure S5 show that in summer at 06:00 GMT, when the wetland was not completely dry (27 June 2015), the T_{air_obs} value of Hasanabad was cooler than its $T_{air_obs_m}$ ($30\text{ }^{\circ}\text{C}$) and Varzaneh with differences of $0.7\text{ }^{\circ}\text{C}$ and $2.1\text{ }^{\circ}\text{C}$, respectively. On these days, there was no wind in Varzaneh. When the wetland was almost completely dry (28 July 2009), the T_{air_obs} value of Hasanabad ($32.1\text{ }^{\circ}\text{C}$) was warmer than that of $T_{air_obs_m}$ and Varzaneh stations with a difference of $2.1\text{ }^{\circ}\text{C}$.

In summer at noontime, when the wetland was not completely dry (27 June 2015), the T_{air_obs} value of Hasanabad was slightly warmer than the $T_{air_obs_m}$ value ($34.5\text{ }^{\circ}\text{C}$) with a difference of $0.1\text{ }^{\circ}\text{C}$ and also cooler than Varzaneh ($35.8\text{ }^{\circ}\text{C}$). While the wetland was completely dry (28 July 2009), the T_{air_obs} value of Hasanabad was $2.5\text{ }^{\circ}\text{C}$ higher than the $T_{air_obs_m}$ value and lower than Varzaneh ($38.2\text{ }^{\circ}\text{C}$), and the air temperature of Varzaneh was $2.1\text{ }^{\circ}\text{C}$ warmer than the $T_{air_obs_m}$ value. On 28 July 2009 and 27 June 2015, at Varzaneh, there were southeasterly and southerly winds at noon (130 and 170 degrees in dry and wet conditions, respectively). Due to the small difference in altitude between Varzaneh and Hasanabad, the wind directions of Hasanabad were considered the same as those of Varzaneh station.

3.3.2. Mann–Kendall Trend Test Results

Figure 7 illustrates the values of Sen's slope ($^{\circ}\text{C}/\text{year}$) of mean monthly minimum and maximum air temperatures (T_{min_m} , T_{max_m}) in three areas: Varzaneh station, Isfahan province, and for all of Iran over a 50-year period (1970 to 2019), a 30-year period before 2000 (1970 to 1999), and 20 years after 2000 (2000 to 2019), respectively. According to Figure 7a,b in all three areas, the slope of T_{max_m} was positive in half of the months (December, January, February, March, May, and October), while the slope of T_{min_m} was positive in all months, and the slope was more significant in Varzaneh than in the province and Iran in most months, i.e., February and April to December with a relatively significant difference (0.02 to $0.06\text{ }^{\circ}\text{C}/\text{year}$). At Varzaneh station, the maximum slope values of T_{max_m} were observed in January (0.07), and then in February (0.06), the maximum slope values of T_{min_m} were related to October (0.1), September and July (0.09) (autumn and summer months).

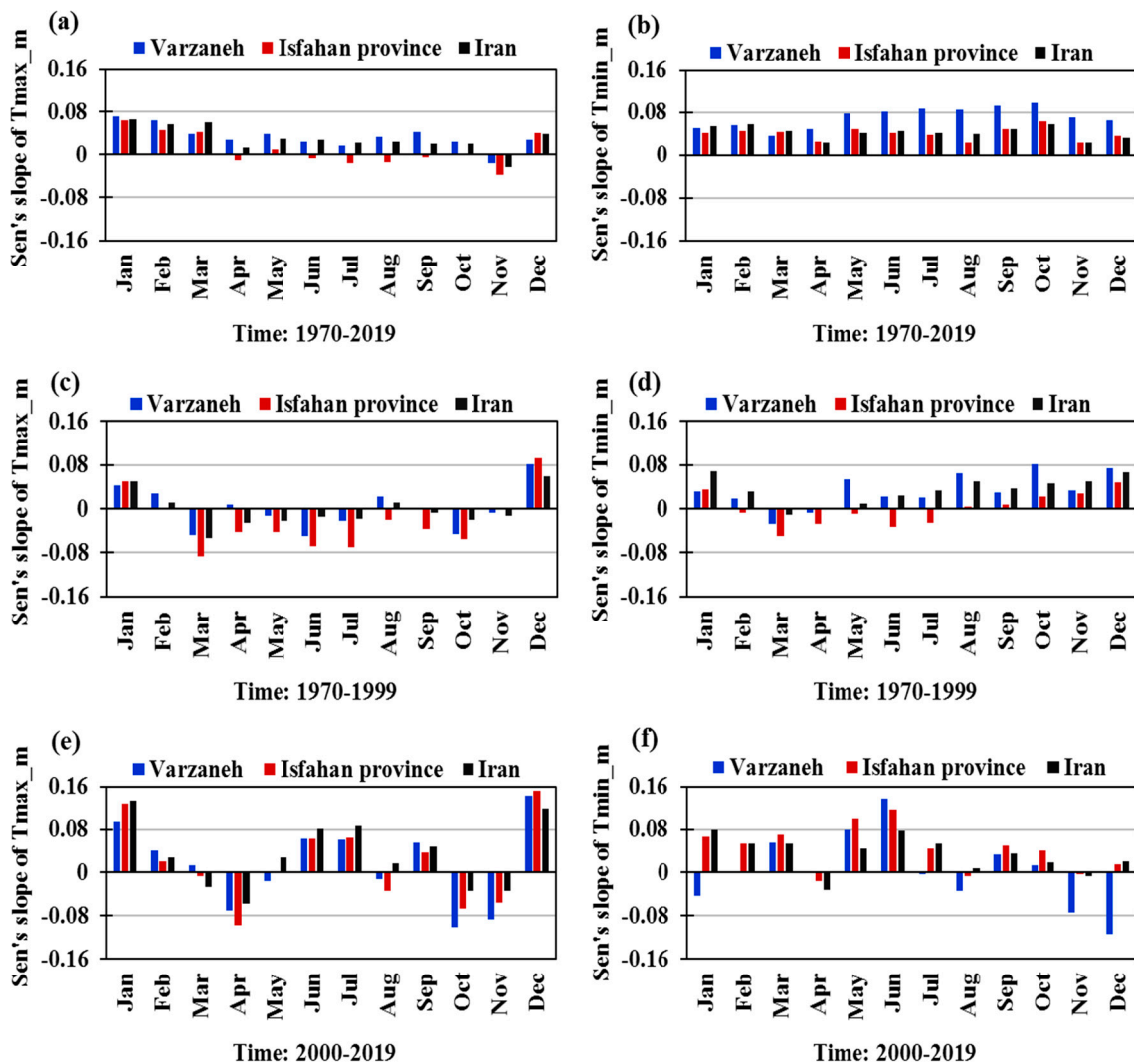


Figure 7. Sen's slope ($^{\circ}\text{C}/\text{year}$) (Mann-Kendall trend) of monthly observed air temperatures ($T_{\text{max_m}}$ and $T_{\text{min_m}}$) at Varzaneh station, Isfahan province, and Iran, for whole period: 1970–2019: (a,b), in the period of 1970–1999: (c,d), and in the period of 2000–2019: (e,f).

In the years before 2000, the rates of change of $T_{\text{max_m}}$ in all three areas were positive only in December, January, and February (generally winter months) and negative in most months. Furthermore, the slope of this temperature was more negative in most months in Isfahan province than in Varzaneh and the country. The slope values of $T_{\text{min_m}}$ were positive in all three areas in six months (August, September, October, November, December, and January) and negative in spring and almost summer months in the province of Isfahan (Figure 7c,d). At Varzaneh station, the slope values of $T_{\text{min_m}}$ in the cold months of the year such as October and December were also higher than those in the province and the country by the difference (0.06, 0.04) and (0.03 and 0.01), respectively (Figure 7c,d), while the slope values in December, January, and November (during the winter) were negative in the post-2000 period (Figure 7e,f).

According to Figure 7e,f, in the 20 years after 2000, the slope values of $T_{\text{max_m}}$ were positive up to half of the months in three areas (generally summer and winter months: December, January, February, June, July, and September), and the rates of $T_{\text{min_m}}$ changes in three areas, in the five months of March, May, June, September, and October were positive, with the magnitude of the slope in Varzaneh being larger than in Isfahan province and Iran only in June (0.02 and 0.06, respectively). Furthermore, the greatest magnitude difference in slope values of $T_{\text{max_m}}$ between Varzaneh with the province and the country were

associated with April (0.03) and March (0.04)–December (0.03), respectively. The greatest magnitude difference in slope values of Tmin_m of Varzaneh with the province and the country were associated with June with values of 0.02 and 0.05, respectively.

3.3.3. *t* Test Results

For performing the *t* test between two groups, the years 1976, 1977, 1978, 1979, 1980, 1987, 1988, 1989, 1993, and 1994 were selected for the wet group, and 2000, 2001, 2002, 2009, 2010, 2011, 2015, 2016, 2017, and 2018 were chosen for the dry group, that showed the Gavkhouni wetland was wet before the year 2000 and has dried up in the recent decades.

Table 3 shows the seasonal mean and *t*-values of Tmin_m and Tmax_m obtained from the two-sample *t* test at Varzaneh station. The difference between the seasonal mean value of Tmax_m when the wetland was dry and when it had water was significant only in spring (March, April, and May) with a value of 1.4 °C ($p < 0.05$ in 2-tailed significance). However, when the wetland was dry, the seasonal mean Tmin_m was significantly increased in most seasons, i.e., winter (December, January, and February), spring (March, April, May), and summer (June, July, and August) with values of 2.64 °C, 1.61 °C, and 1 °C, respectively.

Table 3. The seasonal results of the *t* test for air temperatures between the wet and dry conditions of the Gavkhouni wetland at Varzaneh station.

Temperature	<i>t</i> Test	Winter	Spring	Summer	Autumn
Tmax_m	Mean	−1.43	−1.40	−0.07	−0.68
	<i>t</i>	−1.67	−2.68	−0.21	−1.22
	Sig. (2-tailed)	0.129	0.025 *	0.84	0.252
Tmin_m	Mean	−2.64	−1.61	−1.00	−0.78
	<i>t</i>	−4.70	−5.19	−3.09	−1.42
	Sig. (2-tailed)	−0.001 *	0.001 *	0.013 *	0.189

* Significant at $p \leq 0.05$.

4. Discussion

This study used observed data of temperature and river discharge in combination with remote sensing-based indices and LST to reveal the trend of the Gavkhouni wetland dryness and its impact on the temperature of the surrounding areas. The results show that the drying of the wetland over the last two decades has led to a significant increase in air temperatures in the surrounding areas, especially in the west and northwest in spring and summer seasons.

Since 2000, the smallest wetland extent was observed in 2009, followed by 2011, 2017 and 2015. During all seasons (Figures 6 and S1–S3), LST and air temperature in the Gavkhouni wetland were lower than for the surrounding area, which can be explained by the high albedo of the salt deposits which are exposed during dry periods. In general, water has a low albedo and thus absorbs more incident visible and near-infrared solar radiance. Hence, the albedo increases due to the dryness of the wetland and the salt deposited there, leading to a decrease of LST. Therefore, the wetland cannot balance its ambient temperatures. The values of LST and Tair_calc in the selected years show that the year 2009 was one of the driest years not only in Iran but also in the entire Middle East [50]. The results also indicated a good correlation between LST and Tair_obs ($r^2 = 0.94$, $r = 0.97$) at the stations near the Gavkhouni wetland (Figures S4 and S5). Jafari and Hasheminasab [34] and Shiran et al. [44] also showed that LST variable is a good tool for monitoring arid environments. In addition, the RMSE was by an average of 3 °C, but in general Tair_calc values were consistent with changes in LST for most days and most parts of the studied area. The long-term seasonal average of observed air temperature (Tair_obs_m) at Varzaneh and Hasanabad stations at 06:00 and 12:00 GMT (Table 2) showed that at Hasanabad at 06:00 Tair_obs_m was higher than Varzaneh in all seasons except summer, while at noon it was cooler than Varzaneh station in all seasons. The results of the Mann-Kendall (Sens's slope

estimator) from 1970 to 2019, in general, showed that the slope values of T_{max_m} changes before the year 2000 were often negative, while after the year 2000 were positive in half months. The slope values of T_{min_m} changes in Varzaneh in the period before the year 2000 were higher in the cold months of the year than in the province and the country, while in the last 20 years were lower than the province and the country, which is related to the dryness of the wetland and its failure to play a role in regulating the surrounding temperature. In addition, in the warm months of the year, in the 30 years before and 20 years after 2000, the slope of T_{min_m} changes in Varzaneh station was less and more, respectively, than both the province and country. In the 50 years, the maximum of the slope values of T_{min_m} changes between the three areas were observed in Varzaneh station and months of October (0.1), September (0.09), and July (0.09), also in this period, the maximum difference of the slope of T_{min_m} between Varzaneh and the country ($0.05\text{ }^{\circ}\text{C}/\text{year}$) was related to July (month of summer). On 28 July 2009, when the wetland was in dry conditions, the T_{air_obs} values at Hasanabad and Varzaneh stations at noontime had a difference of $2.5\text{ }^{\circ}\text{C}$ and $2.1\text{ }^{\circ}\text{C}$, respectively, from the long-term average values. To confirm that the wetland dryness affects the climate in the surrounding areas, a t test analysis was used to compare the region's temperature for the dry and wet wetland years. Considering the significant results of the t test for the average of the minimum air temperature in Varzaneh in most seasons, especially in spring and summer (Table 3), and also the Sen's slope results, it can be said that in recent decades with the dryness of the Gavkhouni wetland, the average minimum air temperature in spring and summer has increased by about $1.6\text{ }^{\circ}\text{C}$ and $1\text{ }^{\circ}\text{C}$, respectively. Therefore, from the analysis of the increase in air temperature at Varzaneh and Hasanabad stations on 28 July 2009, It can be concluded that the increase in temperature on this day at noontime was caused not only by global warming but also by the dryness of the Gavkhouni wetland.

In general, the Gavkhouni wetland has been experienced dryness conditions mostly since the 2000s and 2010s decades. According to the NDVI and NDWI results, the negative trend from 1984 to 2020 indicates that the Zayandeh-Rud River has experienced dryness during this period that dried up the Gavkhouni wetland which was a permanent wetland, and the vegetation near the wetland and its entrance decreased. These decreasing trends show that the spectral indices were almost consistent with the other evidence and observed data such as the time series of discharge values at Varzaneh station (Figure 5a,b) which clearly showed the wetland dryness. Besides the drought occurrences, resulted from climate change impact, the human activities in the basin have influenced the drying of the Gavkhouni wetland. Abou Zaki et al. [51] also reported that even in arid and semi-arid climates, water scarcity is mainly due to anthropogenic reasons rather than climate. As presented in other studies, the Gavkhouni wetland dryness is related to population growth and bad management of water resources, such as upstream diversions and unreasonable transmissions of water resources in the basin [42], expansion of agricultural land and irrigation patterns causing hydrological droughts [51], dam construction in upstream of the Zayandeh-Rud River [34]. Related to the remote sensing indices, their accuracy has been confirmed in other studies, such as Eckert et al. [33] and Shiran et al. [44] which indicated that the analysis of NDVI time series can be useful and appropriate to understand the changes in vegetation cover, and also in the study of Jiang et al. [41] which showed the NDVI can accurately indicate the vegetation condition. Abou Zaki et al. [51] also reported that NDWI is a reliable tool for studying the area of surface water bodies.

5. Conclusions

This study was conducted to determine the effects of the Gavkhouni wetland dryness on temperature variations in the surrounding areas. In the last two decades, in addition to global warming impact (such as droughts caused by higher temperatures and evapotranspiration), wetland dryness caused by human activities has led to an increase in air and land surface temperatures in spring and summer, especially in the western and northwestern parts. From 1970 to 2019, the increase in air temperatures in the region was higher than in

the Isfahan province and Iran in general. During the warm months, especially in July, this rate was about 0.02 to 0.06 °C/year higher than the average for Isfahan province and the country. From the current study, it can be concluded that monitoring changes in surface and air temperatures, as well as studying the drying trend of water bodies and their relationship with climate variability in surrounding areas, can be used to develop an integrated plan for managing wetlands and the river that feeds them. The overall results of this study provide a basis for making effective decisions about allocating specific amounts of water to the Gavkhouni wetland to maintain its climate and environmental functions. Considering that many factors such as latitude, cloud cover and direction of prevailing winds affect land surface and air temperatures, it is proposed to use a numerical climate model to improve regional understanding of the impact of wetland dryness on the surrounding climate.

Supplementary Materials: The following are available online at <https://www.mdpi.com/article/10.3390/w14020172/s1>, Figure S1: LST and Tair_calc (°C) variability in the study area in winter: (a) 2009-01-17; (b) 2011-01-07; (c) 2011-01-23; (d) 2017-12-09. Figure S2: LST and Tair_calc (°C) variability in the study area in spring: (a) 2009-05-25; (b) 2011-05-31; (c) 2017-03-12. Figure S3: LST and Tair_calc (°C) variability in the study area in autumn: (a) 2009-10-16; (b) 2011-10-22; (c) 2015-10-17. Figure S4: Linear regression between Landsat LST and Tair_obs values at nearby meteorological stations (Varzaneh and Hasanabad) on the selected 16 days. Figure S5: Tair_calc, Tair_obs and LST values at the meteorological stations on the selected 16 days.

Author Contributions: Conceptualization, H.Y., S.A., M.A.N.-E. and S.P.; Methodology, H.Y., S.A., M.A.N.-E. and S.P.; Validation, S.A., H.Y. and M.A.N.-E.; Investigation, S.A.; Resources, S.A.; Writing—Original Draft Preparation, S.A.; Writing—Review & Editing, S.A., H.Y., M.A.N.-E., W.D. and S.P.; Visualization, S.A.; Supervision, H.Y. and M.A.N.-E. All authors have read and agreed to the published version of the manuscript.

Funding: W.D. received funding from the TU Wien Wissenschaftspreis 2015.

Data Availability Statement: The data presented in this study are available on request from the corresponding author.

Acknowledgments: W.D. acknowledges funding from the TU Wien Science Award 2015. We also would like to thank Rob Weatherby for proof reading and English editing of our paper.

Conflicts of Interest: The authors declare no conflict of interest.

References

- Clarkson, B.R.; Ausseil, A.-G.E.; Gerbeaux, P. Wetland ecosystem services. In *Ecosystem Services in New Zealand: Conditions and Trends*; Manaaki Whenua Press: Lincoln, New Zealand, 2013; pp. 192–202.
- Xu, X.; Chen, M.; Yang, G.; Jiang, B.; Zhang, J. Wetland ecosystem services research: A critical review. *Glob. Ecol. Conserv.* **2020**, *22*, e01027. [[CrossRef](#)]
- Ciężkowski, W.; Szporak-Wasilewska, S.; Kleniewska, M.; Józwiak, J.; Gnatowski, T.; Dąbrowski, P.; Góraj, M.; Szatyłowicz, J.; Ignar, S.; Chormański, J. Remotely Sensed Land Surface Temperature-Based Water Stress Index for Wetland Habitats. *Remote Sens.* **2020**, *12*, 631. [[CrossRef](#)]
- Ramsar Convention Secretariat. *The Ramsar Convention Manual: A Guide to the Convention on Wetlands (Ramsar, Iran, 1971)*; Ramsar Convention Secretariat: Gland, Switzerland, 2013.
- Jing, X.; Qinling, B.; Dan, M. Wetland Monitoring and Land Surface Temperature Response in Panjin City Based on Tiangong-2 Data. In Proceedings of the 2019 2nd International Symposium on Traffic Transportation and Civil Architecture (ISTTCA 2019), Chengdu, China, 13–15 December 2019.
- Carrington, D.P.; Gallimore, R.G.; Kutzbach, J.E. Climate sensitivity to wetlands and wetland vegetation in mid-Holocene North Africa. *Clim. Dyn.* **2001**, *17*, 151–157. [[CrossRef](#)]
- Reidmiller, D.R.; Avery, C.W.; Easterling, D.R.; Kunkel, K.E.; Lewis, K.L.M.; Maycock, T.K.; Stewart, B.C. *Impacts, Risks, and Adaptation in the United States: Fourth National Climate Assessment*; National Oceanic and Atmospheric Administration: Washington, DC, USA, 2017; Volume 2. [[CrossRef](#)]
- Yan, Y.; Mao, K.; Shi, J.; Piao, S.; Shen, X.; Dozier, J.; Liu, Y.; Ren, H.L.; Bao, Q. Driving forces of land surface temperature anomalous changes in North America in 2002–2018. *Sci. Rep.* **2020**, *10*, 6931. [[CrossRef](#)]
- Balew, A.; Korme, T. Monitoring land surface temperature in Bahir Dar city and its surrounding using Landsat images. *Egypt. J. Remote Sens. Space Sci.* **2020**, *23*, 371–386. [[CrossRef](#)]

10. Khandelwal, S.; Goyal, R.; Kaul, N.; Mathew, A. Assessment of land surface temperature variation due to change in elevation of area surrounding Jaipur, India. *Egypt. J. Remote Sens. Space Sci.* **2018**, *21*, 87–94. [[CrossRef](#)]
11. Sekertekin, A. Validation of Physical Radiative Transfer Equation-Based Land Surface Temperature Using Landsat 8 Satellite Imagery and SURFRAD in-situ Measurements. *J. Atmos. Sol. -Terr. Phys.* **2019**, *196*, 105161. [[CrossRef](#)]
12. Sishodia, R.P.; Ray, R.L.; Singh, S.K. Applications of Remote Sensing in Precision Agriculture: A Review. *Remote Sens.* **2020**, *12*, 3136. [[CrossRef](#)]
13. Amiri, R.; Weng, Q.; Alimohammadi, A.; Alavipanah, S.K. Spatial–temporal dynamics of land surface temperature in relation to fractional vegetation cover and land use/cover in the Tabriz urban area, Iran. *Remote Sens. Environ.* **2009**, *113*, 2606–2617. [[CrossRef](#)]
14. Muster, S.; Langer, M.; Abnizova, A.; Young, K.L.; Boike, J. Spatio-temporal sensitivity of MODIS land surface temperature anomalies indicates high potential for large-scale land cover change detection in Arctic permafrost landscapes. *Remote Sens. Environ.* **2015**, *168*, 1–12. [[CrossRef](#)]
15. Li, Y.; Zhao, M.; Motesharrei, S.; Mu, Q.; Kalnay, E.; Li, S. Local cooling and warming effects of forests based on satellite observations. *Nat. Commun.* **2015**, *6*, 6603. [[CrossRef](#)]
16. Chen, Z.; Jiang, W.G.; Tang, Z.H.; Jia, K. Spatial-Temporal Pattern of Vegetation Index Change and the Relationship to Land Surface Temperature in Zoige. In Proceedings of the 2016 XXIII ISPRS Congress, Prague, Czech Republic, 12–19 July 2016; Volume XLI-B3, pp. 849–852. [[CrossRef](#)]
17. Fathizad, H.; Tazeh, M.; Kalantari, S.; Shojaei, S. The investigation of spatiotemporal variations of land surface temperature based on land use changes using NDVI in southwest of Iran. *J. Afr. Earth Sci.* **2017**, *134*, 249–256. [[CrossRef](#)]
18. Hua, A.K.; Ping, O.W. The influence of land-use/land-cover changes on land surface temperature: A case study of Kuala Lumpur metropolitan city. *Eur. J. Remote Sens.* **2018**, *51*, 1049–1069. [[CrossRef](#)]
19. Arekhi, M. Investigating Land Surface Temperature (LST) Change Using the LST Change Detection Technique (Gomishan District, Iran). In *Advances in Remote Sensing and Geo Informatics Applications, Proceedings of the 1st Springer Conference of the Arabian Journal of Geosciences, Sousse, Tunisia, 12–15 November 2018*; Springer: Berlin/Heidelberg, Germany, 2019; pp. 135–139.
20. Rahman, M.M.; Avtar, R.; Yunus, A.P.; Dou, J.; Misra, P.; Takeuchi, W.; Sahu, N.; Kumar, P.; Johnson, B.A.; Dasgupta, R.; et al. Monitoring Effect of Spatial Growth on Land Surface Temperature in Dhaka. *Remote Sens.* **2020**, *12*, 1191. [[CrossRef](#)]
21. Rashid, K.J.; Hoque, M.A.; Esha, T.A.; Rahman, M.A.; Paul, A. Spatiotemporal changes of vegetation and land surface temperature in the refugee camps and its surrounding areas of Bangladesh after the Rohingya influx from Myanmar. *Environ. Dev. Sustain.* **2020**, *23*, 3562–3577. [[CrossRef](#)]
22. Shafizadeh-Moghadam, H.; Weng, Q.; Liu, H.; Valavi, R. Modeling the spatial variation of urban land surface temperature in relation to environmental and anthropogenic factors: A case study of Tehran, Iran. *GISci. Remote Sens.* **2020**, *57*, 483–496. [[CrossRef](#)]
23. Tan, J.; Yu, D.; Li, Q.; Tan, X.; Zhou, W. Spatial relationship between land-use/land-cover change and land surface temperature in the Dongting Lake area, China. *Sci. Rep.* **2020**, *10*, 9245. [[CrossRef](#)]
24. Peng, J.; Ma, J.; Liu, Q.; Liu, Y.; Hu, Y.; Li, Y.; Yue, Y. Spatial-temporal change of land surface temperature across 285 cities in China: An urban-rural contrast perspective. *Sci. Total Environ.* **2018**, *635*, 487–497. [[CrossRef](#)]
25. Mujabar, S.; Rao, V. Estimation and analysis of land surface temperature of Jubail Industrial City, Saudi Arabia, by using remote sensing and GIS technologies. *Arab. J. Geosci.* **2018**, *11*, 742. [[CrossRef](#)]
26. Ezimand, K.; Chahardoli, M.; Azadbakht, M.; Matkan, A.A. Spatiotemporal analysis of land surface temperature using multi-temporal and multi-sensor image fusion techniques. *Sustain. Cities Soc.* **2021**, *64*, 102508. [[CrossRef](#)]
27. Cammalleri, C.; Vogt, J. On the Role of Land Surface Temperature as Proxy of Soil Moisture Status for Drought Monitoring in Europe. *Remote Sens.* **2015**, *7*, 16849–16864. [[CrossRef](#)]
28. Hu, X.; Ren, H.; Tansey, K.; Zheng, Y.; Ghent, D.; Liu, X.; Yan, L. Agricultural drought monitoring using European Space Agency Sentinel 3A land surface temperature and normalized difference vegetation index imageries. *Agric. For. Meteorol.* **2019**, *279*, 107707. [[CrossRef](#)]
29. Zhang, X.; Yamaguchi, Y.; Li, F.; He, B.; Chen, Y. Assessing the Impacts of the 2009/2010 Drought on Vegetation Indices, Normalized Difference Water Index, and Land Surface Temperature in Southwestern China. *Adv. Meteorol.* **2017**, *2017*, 6837493. [[CrossRef](#)]
30. Khan, J.; Wang, P.; Xie, Y.; Wang, L.; Li, L. Mapping MODIS LST NDVI Imagery for Drought Monitoring in Punjab Pakistan. *IEEE Access* **2018**, *6*, 19898–19911. [[CrossRef](#)]
31. Wang, Z.; Guo, P.; Wan, H.; Tian, F.; Wang, L. Integration of Microwave and Optical/Infrared Derived Datasets from Multi-Satellite Products for Drought Monitoring. *Water* **2020**, *12*, 1504. [[CrossRef](#)]
32. Louka, P.; Papanikolaou, I.; Petropoulos, G.P.; Kalogeropoulos, K.; Stathopoulos, N. Identifying Spatially Correlated Patterns between Surface Water and Frost Risk Using EO Data and Geospatial Indices. *Water* **2020**, *12*, 700. [[CrossRef](#)]
33. Eckert, S.; Hüsler, F.; Liniger, H.; Hodel, E. Trend analysis of MODIS NDVI time series for detecting land degradation and regeneration in Mongolia. *J. Arid Environ.* **2015**, *113*, 16–28. [[CrossRef](#)]
34. Jafari, R.; Hasheminasab, S. Assessing the effects of dam building on land degradation in central Iran with Landsat LST and LULC time series. *Environ. Monit. Assess.* **2017**, *189*, 74. [[CrossRef](#)] [[PubMed](#)]

35. Parinussa, R.; Lakshmi, V.; Johnson, F.; Sharma, A. Comparing and Combining Remotely Sensed Land Surface Temperature Products for Improved Hydrological Applications. *Remote Sens.* **2016**, *8*, 162. [[CrossRef](#)]
36. Achmad, A.; Zainuddin; Muftiadi, M. The relationship between land surface temperature and water index in the urban area of a tropical city. In Proceedings of the International Conference on Agricultural Technology, Engineering and Environmental Sciences, Banda Aceh, Indonesia, 21–22 August 2019; Volume 365. [[CrossRef](#)]
37. Eid, A.N.M.; Olatubara, C.O.; Ewemoje, T.A.; El-Hennawy, M.T.; Farouk, H. Inland wetland time-series digital change detection based on SAVI and NDWI indices: Wadi El-Rayan lakes, Egypt. *Remote Sens. Appl. Soc. Environ.* **2020**, *19*, 100347. [[CrossRef](#)]
38. Paul, S.; Pal, S. Predicting wetland area and water depth of Ganges moribund deltaic parts of India. *Remote Sens. Appl. Soc. Environ.* **2020**, *19*, 100338. [[CrossRef](#)]
39. Mukherjee, K.; Pal, S. Hydrological and landscape dynamics of floodplain wetlands of the Diara region, Eastern India. *Ecol. Indic.* **2021**, *121*, 106961. [[CrossRef](#)]
40. Dervisoglu, A. Analysis of the Temporal Changes of Inland Ramsar Sites in Turkey Using Google Earth Engine. *ISPRS Int. J. Geoinf.* **2021**, *10*, 521. [[CrossRef](#)]
41. Jiang, L.; Liu, Y.; Wu, S.; Yang, C. Analyzing ecological environment change and associated driving factors in China based on NDVI time series data. *Ecol. Indic.* **2021**, *129*, 107933. [[CrossRef](#)]
42. Sarhadi, A.; Soltani, S. Determination of water requirements of the Gavkhuni wetland, Iran: A hydrological approach. *J. Arid Environ.* **2013**, *98*, 27–40. [[CrossRef](#)]
43. Mirahsani, M.; Salman Mahini, A.; Soffianian, A.; Moddares, R.; Jafari, R.; Mohammadi, J. Regional Drought Monitoring in Zayandeh-rud Basin Based on Time Series Variations of the SPI and Satellite-Based VCI Indices. *J. Geogr. Environ. Hazards* **2018**, *6*, 1–22. (In Persian)
44. Shiran, M.; Mozzi, P.; Adab, H.; Zangeneh Asadi, M.A. Remote sensing assessment of changes of surface parameters in response to prolonged drought in the arid zone of central Iran (Gavkhoni playa). *Remote Sens. Appl. Soc. Environ.* **2021**, *23*, 100575. [[CrossRef](#)]
45. Molle, F.; Ghazi, I.; Murray-Rust, H. Buying respite: Esfahan and the Zayandeh Rud River basin, Iran. In *River Basin Trajectories: Societies, Environments and Development*; CAB International: Wallingford, UK, 2009; pp. 196–213.
46. Stathopoulou, M.; Cartalis, C. Daytime urban heat islands from Landsat ETM+ and Corine land cover data: An application to major cities in Greece. *Sol. Energy* **2007**, *81*, 358–368. [[CrossRef](#)]
47. Markham, B.L.; Barker, J.L. Spectral characterization of the LANDSAT Thematic Mapper sensors. *Int. J. Remote Sens.* **2010**, *6*, 697–716. [[CrossRef](#)]
48. Weng, Q.; Lu, D.; Schubring, J. Estimation of land surface temperature–vegetation abundance relationship for urban heat island studies. *Remote Sens. Environ.* **2004**, *89*, 467–483. [[CrossRef](#)]
49. Hussain, M.M.; Mahmud, I. pyMannKendall: A python package for non parametric Mann Kendall family of trend tests. *Open Source Softw.* **2019**, *4*, 1556. [[CrossRef](#)]
50. Amini, A.; Zareie, S.; Taheri, P.; Yusof, K.B.W.; ul Mustafa, M.R. Drought Analysis and Water Resources Management Inspection in Euphrates–Tigris Basin. In *River Basin Management*; IntechOpen: Rijeka, Croatia, 2016.
51. Abou Zaki, N.; Torabi Haghighi, A.; Rossi, P.M.; Tourian, M.J.; Bakhshae, A.; Kløve, B. Evaluating Impacts of Irrigation and Drought on River, Groundwater and a Terminal Wetland in the Zayanderud Basin, Iran. *Water* **2020**, *12*, 1302. [[CrossRef](#)]